



Fabrication of ordered mesoporous carbons with tunable pore architecture by the cosolvent

Peng Li¹ · Xiaoxiao Ma^{1,2} · Yanliang Zhao¹ · Junhua Tan¹ · Fei Liu¹ · Kaijin Zhu¹

Published online: 2 January 2019
© Springer Science+Business Media, LLC, part of Springer Nature 2019

Abstract

Ordered mesoporous carbons (OMCs) with tunable mesophase were prepared by a novel cosolvent method using low molecular resin as carbon precursor, and P123(Poly(ethyleneoxide)-poly(propyleneoxide)-poly(ethyleneoxide)triblock copolymers, EO₂₀PO₇₀EO₂₀) as a template via an Evaporation-induced Self-assembly Process (EISA). The results show that the pore structure of OMCs could be oriented from 2D hexagonal (p6mm) to 2D centered rectangular (C2mm) structure. Two key descriptors of mesophase were identified. One is the ratio of PEO/PPO of triblock copolymer, and the other one is cosolvent, both of which would have effects on the interface of mesophase during the EISA process. Furthermore, it was confirmed that the ordered mesophase could be obtained in a very short time during the EISA process even accompanied by the micro-emulsion phenomenon.

Keywords Ordered mesoporous carbons · Mesophase · PEO/PPO · Cosolvent strategy

1 Introduction

Ordered mesoporous carbons (OMCs) have been attracting numerous attention due to their unique properties such as high ordered arrangement of mesopore, large pore volume, large surface area, narrow pore size distribution, high chemical stability and high conductivity [1–3]. Therefore, OMCs have great potential application ranging from energy and storage [4] to large molecular [5] or polluted metal ion adsorption [6] and to catalysis and so on [7]. Pore structure of ordered mesoporous materials is very important when considered their practical application [8, 9]. Take two dimensional (2D) hexagonal (p6mm) mesopore structure as an example, the straight channel like mesopore structure with large pore volume, which is popular for fast transportation [10, 11] and adsorption of chemical pollutants [12, 13]. In addition, three dimensional (3D) cubic OMCs exhibited superior specific capacitance compared with other OMCs [14].

Up to now, there are two main methods to synthesize OMCs [15]. The one is nanocasting technique usually with pre-synthesized ordered mesoporous silica or highly packed inorganic metal oxides, which is very powerful to synthesize OMCs with controllable pore morphology and pore size [16–19]. However, this technique brings a serious burden to the sustainable environment owing to the cost of the specific template and the toxic chemicals such as HF in addition to the time consuming production process. Soft-template method, the other one was developed under this context. This technique emerged as a more popular strategy to synthesize OMCs because of the simple and easy operation only employing resin as carbon precursor and copolymer as template [20–23]. Via this strategy, OMCs with monolith [24], fiber [25], film [26, 27], sphere [28] and single crystals [20] were successfully achieved.

Up to now, although various OMCs with various mesophase have been achieved, highly suitable carbon precursors and soft template should be selected. Compared with mesophase of ordered mesoporous silica, the fabrication of mesophase of OMCs is still a challenge. Control of mesophase of OMCs usually was achieved by carefully selected the precursors and suitable template [29]. The cosolvent or additives are very important in fabrication of mesophase [30]. There was also some work on the synthesis of OMCs in ethanol–water phase through phase separation strategy

✉ Peng Li
nkpengli@mail.nankai.edu.cn

¹ Department of Materials Engineering, Taiyuan Institute of Technology, Taiyuan 030008, Shanxi, China

² School of Materials Science and Engineering, North University of China, Taiyuan 030051, China

[31, 32]. However, only a few of papers focusing on tailoring the mesophase of OMCs by an Evaporation-induced Self-assembly Process (EISA) [33]. Therefore, a novel method of tuning the mesophase of OMCs was developed using the P123 as the template and low resin via the EISA process using water as the cosolvent as shown in Fig. 1.

2 Experimental

2.1 Chemicals

Poly(ethylene oxide)-poly(propylene oxide)-poly(ethylene oxide) triblock copolymers [(P123) $\text{EO}_{20}\text{PO}_{70}\text{EO}_{20}$, $M_w = 5800$; (F127) $\text{EO}_{106}\text{PO}_{70}\text{EO}_{106}$, $M_w = 12,600$] were purchased from BASF Corp. phenol, formalin solution (37–40 wt%), NaOH and ethanol were purchased from Tianjin Chem Corp. All chemicals were used as received without further purification.

2.2 Preparation of OMCs

The typical process of OMCP proceeds as follows: P123 (1 g) was dissolved in mixture of ethanol (20-X ml) and cosolvent water (X ml) under magnetic stirring at 30 °C. Then, first, the solvable 1 g of phenol was melted at 45 °C before 0.2 g of NaOH aqueous (20 wt%) was added into with stirring. 2.2 g of formalin (37–40 wt%) was added dropwise, and the mixture was stirred at 75 °C for 60 min. After cooling the mixture to room temperature, the pH of the reaction was adjusted to neutral (7.0) using 2.0 M HCl aqueous solution. Water was then removed under vacuum below 50 °C for 2 h, then resin was diluted to 1 g resin/20 ml ethanol. Subsequently, the resin solution was added into the ethanol solution containing P123, and stirred for 10 min to form a homogeneous solution. A light yellow film was obtained by pouring the solution into a dish and evaporated at room temperature over 24 h, then heating in an oven at 100 °C for 24 h. OMCP-X was obtained by direct carbonization of the

as synthesized samples at 800 °C for 2 h at a heating rate of 1 °C min^{-1} under N_2 (here the samples were nominated as OMCP-X, where X was corresponding to the volume of the cosolvent). For comparison, samples with F127 as template under the same condition were also prepared, denoted as OMCFs-X.

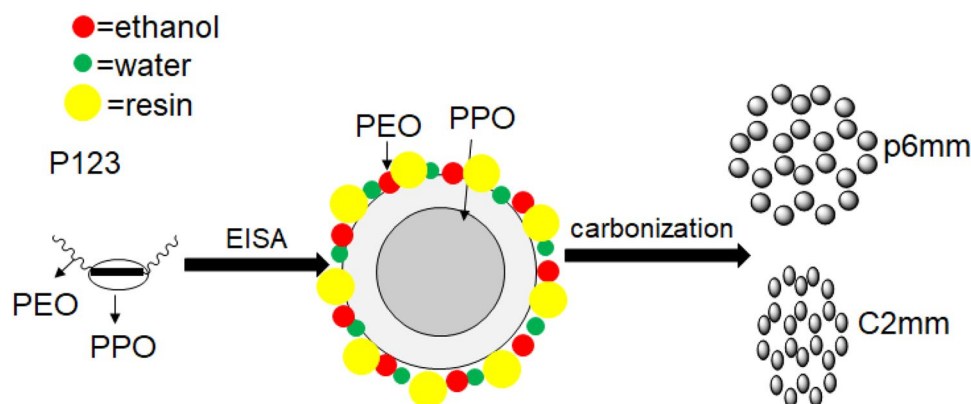
2.3 Characterization of OMCs

Small-angle X-ray scattering (SAXS) recorded by using an imaging plate with X-ray wavelength of λ 1.38 Å at beam line 4B9A of the Beijing Synchrotron Radiation Facility (BSRF). TEM measurement was conducted using a Hitachi H-800. Nitrogen adsorption–desorption isotherms were performed at 77 K on a TriStar 3000 volumetric adsorption system. The Brunauer–Emmett–Teller (BET) model was adopted when calculated the specific surface area. Barrett–Joyner–Halenda (BJH) method was used to obtain the pore size distribution curve. The total pore volume (V_{total}) was calculated at the relative pressure of 0.99. The micropore volume (V_{micro}) was determined by t-plot model, and the mesoporous volume (V_{meso}) was calculated by the difference of V_{total} and V_{micro} .

3 Results and discussion

Figure 2 shows the SAXS patterns of the obtained OMCP. It could be seen that mesophase of OMCP-X varies with the increasing amount of cosolvent water. For the completely pure ethanol solvent, the OMCP-0 presented 2 peaks which could be indexed to the (100) and (110) directions of p6mm pore symmetry. Interestingly, it could be observed that the SAXS patterns of OMCP-3, OMCP-8 and OMCP-9 shown a series of peaks which could be described as the (11), (20) and (02) planes of the C2mm [34], indicating that the mesophase had changed from the p6mm to C2mm with the increasing of the amount the cosolvent water. Noticeably, when the cosolvent of hexane reach as high as 11 ml,

Fig. 1 Schematic representation of preparation of OMCP



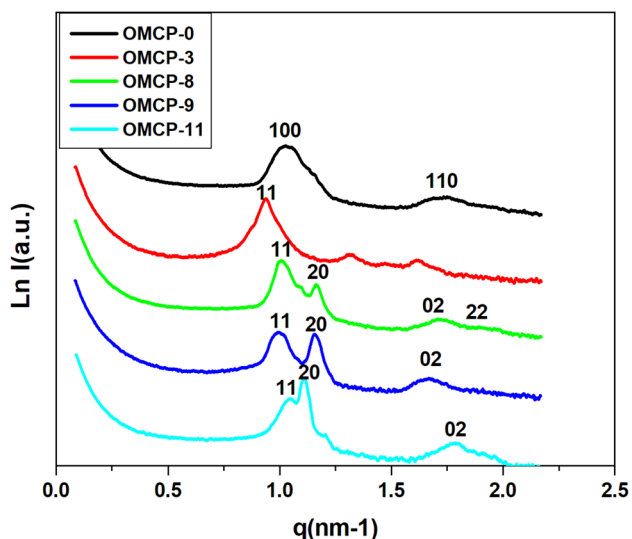


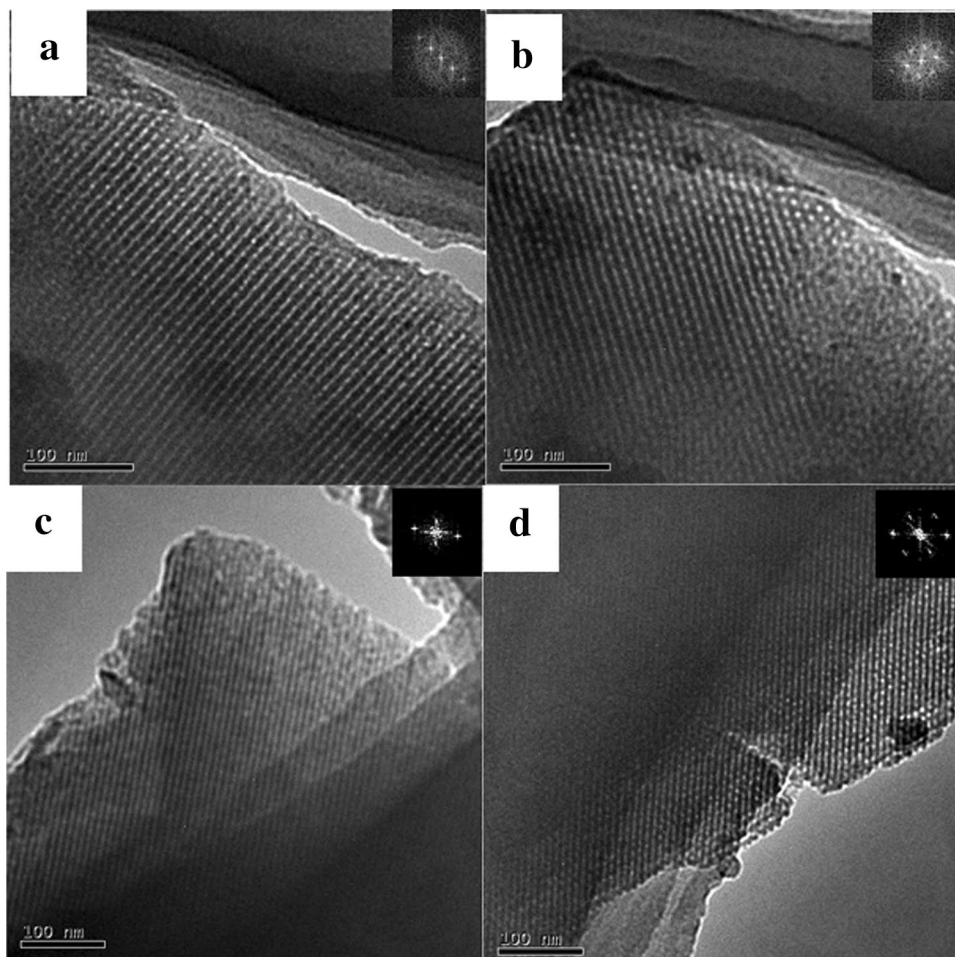
Fig. 2 SAXS patterns of the OMCP-X

the system became microemulsion once the resin solution added into. Even though, the ordered mesophase of

OMCP-11 could be kept in the microemulsion system, further confirmed the fast formation of mesophase during the EISA process. For comparison, All the ordered mesoporous carbons synthesized using F127 as template (OMCF) had mesophase changing from Im3m (OMCF-0, 3, 11) to C2mm (OMCF-14, 16) and back to Im3m (OMCF-18, 19) symmetry again various cosolvent water (SI) [35]. It was found that mesophase of OMCF did not change until the water amount reached as high 14 ml. In addition, the mesophase of returned to Im3m when the water content was high to 18 or 19 ml. The reason why OMCP and OMCF had obvious difference is the different ratio of PEO/PPO. The F127 has the long hydrophilic PEO part and high solubility in water solvent, so when water was used as the cosolvent, it did not affect the formation of mesophase remarkably compared with that of P123.

Figure 3 shows the TEM images and FFT calculations of typical OMCP samples with mesophase varied with the increasing amount of cosolvent. As shown in the Fig. 3a, b, TEM images of OMC-0 exhibited the channel-like array and hexagonal pore structure along the (110) and (100), further confirming the 2D hexagonal symmetry. With the cosolvent

Fig. 3 TEM images of OMCP-0 (a, b), OMCP-9 (c, d), insets are the Fast Fourier Transformations (FFT) of the corresponding pictures



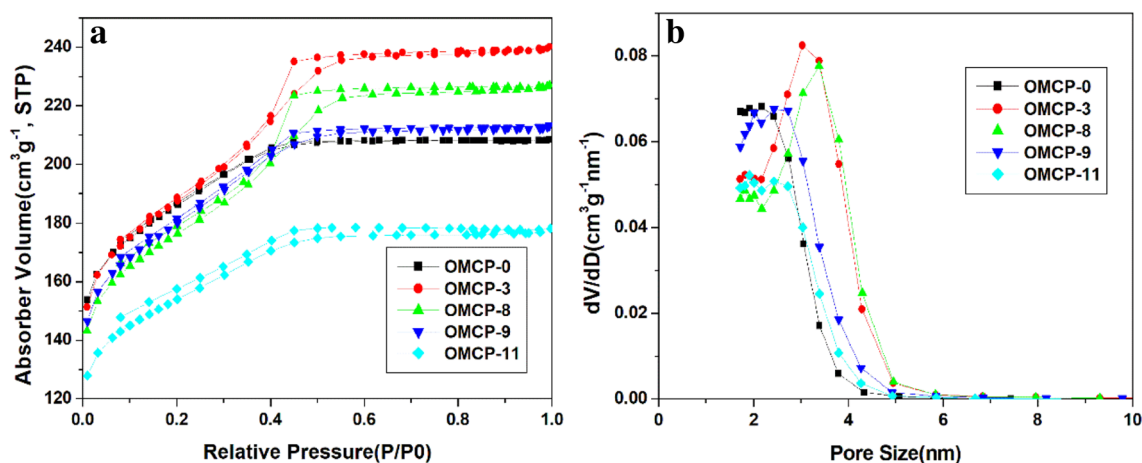


Fig. 4 N_2 adsorption/desorption isotherms (a) and BJH pore size distribution curve (b) of the OMCP-X

Table 1 Parameters of the MCs-X

Sample	S_{BET} (m ² /g)	Pore size (nm)	V_{total} (cm ³ /g)	V_{micro} (cm ³ /g)	V_{meso} (cm ³ /g)	Ratio _{meso} (%)
OMCP-0	590	2.2	0.32	0.18	0.14	50
OMCP-3	600	3.0	0.37	0.17	0.20	54
OMCP-8	563	3.4	0.35	0.16	0.19	54
OMCP-9	576	2.4	0.33	0.16	0.17	52
OMCP-11	488	1.9	0.28	0.15	0.13	46

$$\text{Ratio}_{\text{meso}} = (V_{\text{total}} - V_{\text{micro}}) / V_{\text{total}}$$

water increasing to 9 ml, the stripe pore structure of TEM images could be observed clearly and distorted hexagonal mesopore (Fig. 3c, d) of OMCP-9, suggesting that OMCP-9 has a 2D centered rectangular symmetry.

The nitrogen adsorption and desorption isotherms of OMCP-X (Fig. 4a) and pore size distribution (Fig. 4b) were shown in Fig. 4. All samples show the type-IV curves with obvious hysteresis, which are typical characterizations of mesoporous materials. There was an interesting that the adsorption pore volume increases when not too much cosolvent water used. As the amount of water increased, the pore volume decreased possibly of the distortion of pore structure long the hexagonal direction. The OMCP-11 has the least pore volume maybe because of the microemulsion phenomenon of system (Table 1). The pore size distributions of all samples are uniform centered at about 2.1–3.5 nm as shown in Fig. 4b.

4 Conclusion

Water was adopted as cosolvent to fabrication of mesophase of OMCs via an EISA strategy. The results show that the pore structure of OMCs could be oriented from

2D hexagonal (p6mm) to 2D centered rectangular C2mm structure. The curvature of mesophase interface could be decided by two factors. One is the ratio of PEO/PPO of triblock copolymer, and the other one is cosolvent. The F127 with long hydrophilic PEO part could withstand much more cosolvent than that of P123 with short hydrophilic PEO chain. Moreover, it was confirmed that the ordered mesophase could be obtain in a very short time during the EISA process even accompanied by the microemulsion process.

Acknowledgements The research was supported by the financial support of the Shanxi Province Foundation for Youths (2015021072), the Program for the Innovative Talents of Taiyuan Institute of Technology (TITXD201403), Special Youth Science and Technology Innovation (QKCZ201635), National Training Programs of Innovation and Entrepreneurship for Undergraduates (201614101004), the Fund for Shanxi “1331 Project” Key Subjects Construction and greatly thanks Fund of Testing from Institute of High Energy and Physics for SAXS measurements assistance.

References

1. S. Abouali, M. Akbari Garakani, J.K. Kim, *Electrochim. Acta* **284**, 436–443 (2018)

2. J. Deng, X. Yu, X. Qin, B. Liu, Y.B. He, B. Li, F. Kang, *Energy Storage Mater.* **11**, 184–190 (2018)
3. C. Liang, S. Dai, *J. Am. Chem. Soc.* **128**, 5316–5317 (2006)
4. H. Chen, Q. Li, N. Teng, D. Long, C. Ma, Y. Wei, J. Wang, L. Ling, *Electrochim. Acta* **214**, 231–240 (2016)
5. X. Peng, F. Hu, J. Huang, Y. Wang, H. Dai, Z. Liu, *Microp. Mesopor. Mater.* **228**, 196–206 (2016)
6. F. Liu, Z. Guo, H. Ling, Z. Huang, D. Tang, *Microp. Mesopor. Mater.* **227**, 104–111 (2016)
7. W. Xu, Z. Wu, S. Tao, *J. Mater. Chem. A* **4**, 16272–16287 (2016)
8. Y. Liang, Z. Li, X. Yang, R. Fu, D. Wu, *Chem. Commun.* **49**, 9998–10000 (2013)
9. A.H. Lu, G.P. Hao, Q. Sun, X.Q. Zhang, W.C. Li, *Macromol. Chem. Phys.* **213**, 1107–1131 (2012)
10. Q. Shi, R. Zhang, Y. Lv, Y. Deng, A.A. Elzatahry, D. Zhao, *Carbon*, **84**, 335–346 (2015)
11. Y. Liang, Z. Li, R. Fu, D. Wu, *J. Mater. Chem. A* **1**, 3768–3773 (2013)
12. M. Barczak, K. Michalak-Zwierz, K. Gdula, K. Tyszczyk-Rotko, R. Dobrowolski, A. Dąbrowski, *Microporous Mesoporous Mater.* **211**, 162–173 (2015)
13. C. He, X. Hu, *Ind. Eng. Chem. Res.* **50**, 14070–14083 (2011)
14. D. Zhang, L. Zheng, Y. Ma, L. Lei, Q. Li, Y. Li, H. Luo, H. Feng, Y. Hao, *ACS. Appl. Mater. Interface* **6**, 2657–2665 (2014)
15. M. Enterría, J.L. Figueiredo, *Carbon* **108**, 79–102 (2016)
16. D. Zhang, M. Han, Y. Li, B. Wang, K. Wang, Y. Wang, T. Yang, J. He, H. Feng, *J. Porous. Mater.* **25**, 29–35 (2017)
17. R. Ryoo, S.H. Joo, S. Jun, *J. Phys. Chem. B* **103**, 7743–7747 (1999)
18. A. Sánchez-Sánchez, V. Fierro, M.T. Izquierdo, A. Celzard, *J. Mater. Chem. A* **4**, 6140–6148 (2016)
19. G.P. Mane, S.N. Talapaneni, K.S. Lakhi, H. Ilbeygi, U. Ravon, K. Al-Bahily, T. Mori, D.-H. Park, A. Vinu, *Angew. Chem. Int. Ed.* **56**, 8481–8485 (2017)
20. H. Tan, J. Tang, X. Zhou, D. Golberg, S.K. Bhatia, Y. Sugahara, Y. Yamauchi, *Chem. Commun.* **54**, 9494–9497 (2018)
21. P. Li, Y. Song, Q. Lin, J. Shi, L. Liu, L. He, H. Ye, Q. Guo, *Microp. Mesopor. Mater.* **159**, 81–86 (2012)
22. P.W. Xiao, L. Zhao, Z.-Y. Sui, M.Y. Xu, B.-H. Han, *Microp. Mesopor. Mater.* **253**, 215–222 (2017)
23. H. Wang, W. Wang, M. Asif, Y. Yu, Z. Wang, J. Wang, H. Liu, J. Xiao, *Nanoscale* **7**, 15534–15541 (2017)
24. G. Hasegawa, K. Kanamori, T. Kiyomura, H. Kurata, T. Abe, K. Nakanishi, *Chem. Mater.* **28**, 3944–3950 (2016)
25. N. Liu, H. Song, X. Chen, *J. Mater. Chem.* **21**, 5345–5351 (2011)
26. Q. Zhang, F. Matsuoka, H.S. Suh, P.A. Beaucage, S. Xiong, D.M. Smilgies, K.W. Tan, J.G. Werner, P.F. Nealey, U.B. Wiesner, *ACS Nano* **12**, 347–358 (2017)
27. G. Deng, Y. Zhang, C. Ye, Z. Qiang, G.E. Stein, K.A. Cavicchi, B.D. Vogt, *Chem. Commun.* **50**, 12684–12687 (2014)
28. M. Zhao, D.-L. Zhao, X.-Y. Han, H.-X. Yang, Y.-J. Duan, X.M. Tian, *Electrochim. Acta* **287**, 21–28 (2018)
29. T.Y. Ma, L. Liu, Z.Y. Yuan, *Chem. Soc. Rev.* **42**, 3977–4003 (2013)
30. H. Sai, K.W. Tan, K. Hur, E. Asenath-Smith, R. Hovden, Y. Jiang, M. Riccio, D.A. Muller, V. Elser, L.A. Estroff, S.M. Gruner, U. Wiesner, *Science* **341**, 530–534 (2013)
31. J. Gorka, C. Fenning, M. Jaroniec, *Colloids Surf. A* **352**, 113–117 (2009)
32. J. Choma, K. Jedynek, M. Marszewski, M. Jaroniec, *Adsorption* **19**, 563–569 (2013)
33. P. Li, Y. Song, Z. Tang, G. Yang, Q. Guo, L. Liu, J. Yang, *J. Colloid Interface Sci.* **401**, 161–163 (2013)
34. D. Zhao, Q. Huo, J. Feng, J. Kim, Y. Han, G.D. Stucky, *Chem. Mater.* **11**, 2668–2672 (1999)
35. C.M. Yang, C.Y. Lin, Y. Sakamoto, W.C. Huang, L.L. Chang, *Chem. Commun.* **45**, 5969–5971 (2008)